ADVANCED FUNCTIONAL MATERIALS
www.afm-journal.de

"Nano-Fishnet" Structure Making Silk Fibers Tougher

Ruchuan Liu, Qinqiu Deng, Zhen Yang, Daiwen Yang, Ming-Yong Han, and Xiang Yang Liu**

Based on the combined technologies of atomic force microscopy, X-ray diffraction/scattering, Fourier transform infrared spectra analysis, etc., it is demonstrated that the nano-fishnet-like networks, one of the most flexible but toughest structures, turn out to be the basic structure of silk filaments. The force patterns of pulling individual fibrils allow the identification of the pathways of unfolding protein segments in stacking β-crystallites, which reveal the fishnet-like topology. The calculation shows that the β-crystallites in silk nanofibrils are the cross-linking points of the nano-fishnets, which may enhance the toughness of silk filaments up to 1000 times, compared with amyloid-like and unlinked string structures. It follows that the strong β-sheet–β-sheet interaction, a high degree of ordering, and a high density of β-crystallites in silk fibers toughen the fishnet structure, then strengthen silk filaments, in consistency with the experiments for both spider and silkworm silks. The knowledge on the fishnet structure of silk fibers sheds light on the design and synthesis of either protein or synthetic fibers of ultraperformance in a more generic way.

1. Introduction

Nowdays, soft materials become increasingly important due to the applications in flexible electronics, photonics, and biomedicines.[1] The mesoscale phenomena and architectures of soft materials are essential in generating the next generation of technology opportunities, societal benefits, and scientific advances.[2] The accumulating facts indicate that the functionality of soft materials that is critical to macroscopic performance begins to manifest itself not at the atomic or nanoscale but at the mesoscale.[3]

Animal silks, including both spider and silkworm silks, show the hierarchical structures of amorphous chains and stacked β-sheets.[4] Due to the unique mechanical, optical, and biological behavior,[5] silk materials are found to have a broad range of applications in tissue engineering, bioelectronics, optics, and other areas.[6] In particular, the toughness of spider dragline silk fibers overrides Kevlar, steel, and most man-made fibers available today.[6c,7] The most recent studies reveal that both spider dragline and silkworm silk fibers consist of bundles of twisted nanofibrils,[2,8] which in turn consist of amorphous molecular chains and β-sheet nanocrystallites.[4a,9] The great mechanical strength and substantial elasticity of silk fibers are believed to be in connection with a special arrangement of amorphous molecular chains and β-sheet nanocrystallites in nanofibrils.[4a,7c,10] Unfortunately, although there are a number of speculations concerning such an arrangement,[4a,g,7c,10a,11] none of them have been directly verified experimentally.

As a type of soft materials, the performance of silk fibers should also be determined by four factors of hierarchical network structures (**Figure 1**):[2,12]

(1) Topology: The topology of nodes describes how the joints/points are associated with each other.
(2) Correlation length: The average of the distance between two adjacent building blocks in the same structural level.
(3) Ordering/symmetry of building blocks: The symmetry or ordering of the nodes (or the representing blocks) of the network structure determine the performance of the materials.
(4) Strength of linkage or interactions: It refers to the strength of linkage or interactions between the adjacent structural units at the same level. The linkage can be physical, chemical bonding, or virtual connection/association.[13]

We notice that animal silks as a class of soft materials have been found having a wide range of applications.[14] Among those, nanoarchitectures assembled by stacked β-sheets of

Prof. R. Liu, Dr. Z. Yang, Prof. X. Y. Liu
Research Institute for Biomimetic and Soft Matter
Fujian Provincial Key Lab for Soft Functional Research
Xiamen University
Xiamen 361005, P. R. China
E-mail: phyliurc@cqu.edu.cn; phyliuxy@nus.edu.sg
Prof. R. Liu, Prof. X. Y. Liu
Department of Physics
National University of Singapore
2 Science Drive 3, Singapore 117551, Singapore
Prof. R. Liu
School of Physics
Chongqing University
Chongqing 401331, P. R. China
Dr. Q. Deng, Prof. X. Y. Liu
NUS Graduate School for Integrative Sciences and Engineering
National University of Singapore
28 Medical Drive, Singapore 117456, Singapore
Prof. D. Yang
Department of Biological Sciences
National University of Singapore
14 Science Drive 4, Singapore 117543, Singapore
Prof. M.-Y. Han
Institute of Materials Research and Engineering
2 Fusionopolis Way, Singapore 138634, Singapore

DOI: 10.1002/adfm.201600813

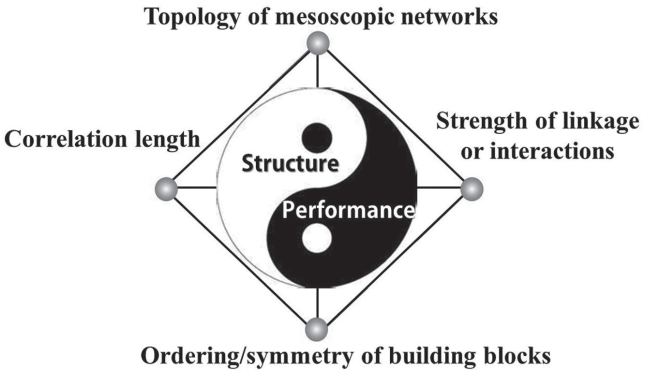

Figure 1. Scheme illustrating the four factors describing the performance of silk materials in relationship with the mesoscopic structure.

proteins/peptides, e.g., silk fibrils, possess prominent mechanical stability,[15] which can be credited to the strength of stacked β-sheets and the nanonetwork topology in their connections. On one hand, to investigate the nanostructures of these biomolecules, X-ray diffraction (XRD),[16] electron microscopy,[17] nuclear magnetic resonance (NMR),[18] Fourier transform infrared spectra (FTIR),[19] and Raman spectroscopy[19b] have been adopted. On the other hand, the details of the hierarchical structure of silk fibrous materials and the correlation with the mechanical performance have not been obtained yet. In other words, what makes silk fibers, in particular, spider dragline silk fibers so tough remains unclear. Atomic force microscopy (AFM) instrumentation emerges as a powerful technique to probe nanostructures and the corresponding nanomechanics of protein-based nanostructures.[20] While the surface properties are measured with a high spatial resolution, the nanomechanical properties of individual fibrils[11,21] of stacked β-sheets can be unraveled, including Young's moduli[22] and unfolding forces of the secondary structures.[21d,e,23] Furthermore, the nanonetwork topology, i.e., how the secondary structure units are associated to construct networks in silk nanofibrils, seem to be determined solely by AFM.

In this paper, we will apply the soft matter mesoscopic structure-performance Yin-Yang sphere model (Figure 1)[2,12] to examine how the mesoscopic structures of both spider and silkworm silk molecules are arranged at the fibril scale, and why the fishnet structure can give rise to the usual mechanical performance of silk fibers consequently. To achieve this goal, we will take advantage of the unique functions of AFM force spectroscopy in combination with Small-angle X-ray scattering (SAXS), FTIR, and XRD spectra, to acquire the particular arrangement of amorphous molecular chains and β-sheet nanocrystallites in silk nanofibrils on silk fibrils, furthermore, we will further explore how the arrangement of fishnet structure can give rise to the usual mechanical performance of silk fibers consequently. This will also provide a new approach to measuring and analyzing molecular network structures directly.

2. Results and Discussion

2.1. Decoding the Topology of the Mesoscopic Structure of Silk Fibrils

In this study, silkworm *Bombyx mori* (*B. mori*) cocoon silk (BMCS) and spider *Nephila antipodiana* eggcases silk (NAES) fibrils acquired from their silk protein solutions were examined in detail. Later, the discussion will also be extended to spider *N. pilipes* dragline silk (NPDS) fibers. The results from AFM topography, SAXS, FTIR, and XRD spectra confirm the structural similarities between regenerated BMCS fibrils and the natural silk fibers (**Figure 2** and Note 1 (Supporting Information)), which enable us to use individual regenerated BMCS nanofibrils as a surrogate for natural silk fibers in structural characterization by AFM force mode, and this is of critical importance.

We notice that there are three possibilities in connecting β-crystallites into a network by amorphous chains: (1) a fishnet structure with β-crystallites as the nodes, (2) a more ordered slab-segment structure as proposed by Oroudjev et al.,[11] or (3) a molecular network as in amyloid fibrils.[24] In the following, regenerated BMCS fibrils were adopted to verify the network

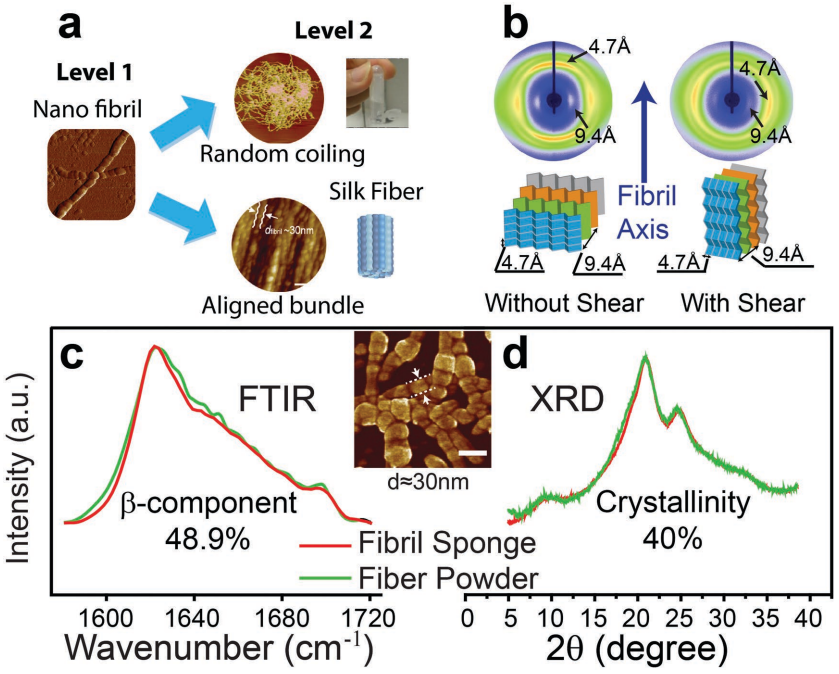

Figure 2. The hierarchical structure of BMCS natural fibrils and fibers and regenerated fibrils. a) The two levels of the hierarchical structure of silkworm silk materials. A silk fiber is a huddle of silk fibrils. b) XRD patterns of β-crystals in silk fibrils folded into either parallel or cross to the fiber axis arrangement, tuned by shear force. In the natural fibers, the β-crystals of silk fibrils acquired under shear are the same as silk fibers. c) The FTIR spectra and d) X-ray diffraction spectra. Inset in (c) is an AFM image of regenerated BMCS fibrils, and the diameter is ≈30 nm. (Scale bar, 50 nm)

Adv. Funct. Mater. **2016**,
DOI: 10.1002/adfm.201600813

type in terms of AFM force spectroscopy. In this regard, the examination of network type will be focused on the unfolding of nano-β-crystallites and the critical stress bearing units in the networks, and the topology at the points. The analysis will show how the nano-β-crystallites are associated with each other in the nanofibrils, and how the breakage occurs under stretching.

In the experiments, individual silk nanofibrils were first localized by AFM imaging. Then the AFM tip was used to pull each fibril to probe the elasticity of the β-crystallites.[11] In addition, the way that the silk protein chains are connected by β-crystallites can significantly affect the dissipation of the force from the AFM tip among the semicrystalline networks, and this can be reflected by the measured force patterns.

Typical saw-tooth patterns are observed in the force versus extension trajectories of regenerated BMCS fibrils (**Figure 3**a,b). In these force patterns, the height of the force peaks corresponds to the strength of hydrogen-bonds (H-bonds) or the inter-β-sheet interactions in β-crystallites, while the extension changes between force peaks correspond to the length of the β-strand/β-sheet plus the amorphous chain next to it. Most trajectories (94%) exhibit sequential unfolding events of random peak forces with no clear trend (Figure 3a). The rest force–extension trajectories (6%) display a characteristic pattern: the highest unfolding force peak followed by a series of events showing a general upward trend in unfolding forces (Figure 3b). These are different from the characteristic plateau force patterns observed for amyloid fibrils,[23b,c] indicating the dissimilar molecular network structure in silk fibrils. This disparity is consistent with the results from XRD spectra: the β-strands in crystallites are aligned along the fibril axis, unlike in the case of amyloid fibrils.[24]

To identify the topology of the networks, two possible pathways to unfold the β-strands from β-crystallites can be distinguished: (pathway 1) to sequentially unzip β-strands directly from a β-crystallite (Figure 3c), or (pathway 2) to peal a β-sheet off a crystallite first, then unzip β-strands from the peeled off β-sheet (Figure 3d). In the first pathway, at each step of unzipping β-strands, the force is mostly applied onto the β-strand through the chain connecting to the AFM tip, while other strands in the β-crystallite share the force due to the integrated response of the β-crystallite. Thus, the β-strand at the force point experiences a force much higher than others, so is unzipped first. This is followed by the next one in the molecular chain. As the strength of each β-strand is different, the consequent force pattern shows peaks of random heights (Figure 3a). This is similar to the case of pulling transmembrane proteins.[25]

Concerning on the interconnection of β-crystallites, the consequent force patterns will be different. In the case of the slab-segment model,[11] the force distribution among the β-strands in the β-sheet is similar to that in β-crystallites, and a force pattern similar to that of the first pathway is expected. However, when the β-crystallites are cross-linked with each other as in a "fishnet", a β-sheet out of a β-crystallite is then stretched between two anchor points: between the AFM tip and the β-crystallite. It follows that the stretching force can be exerted

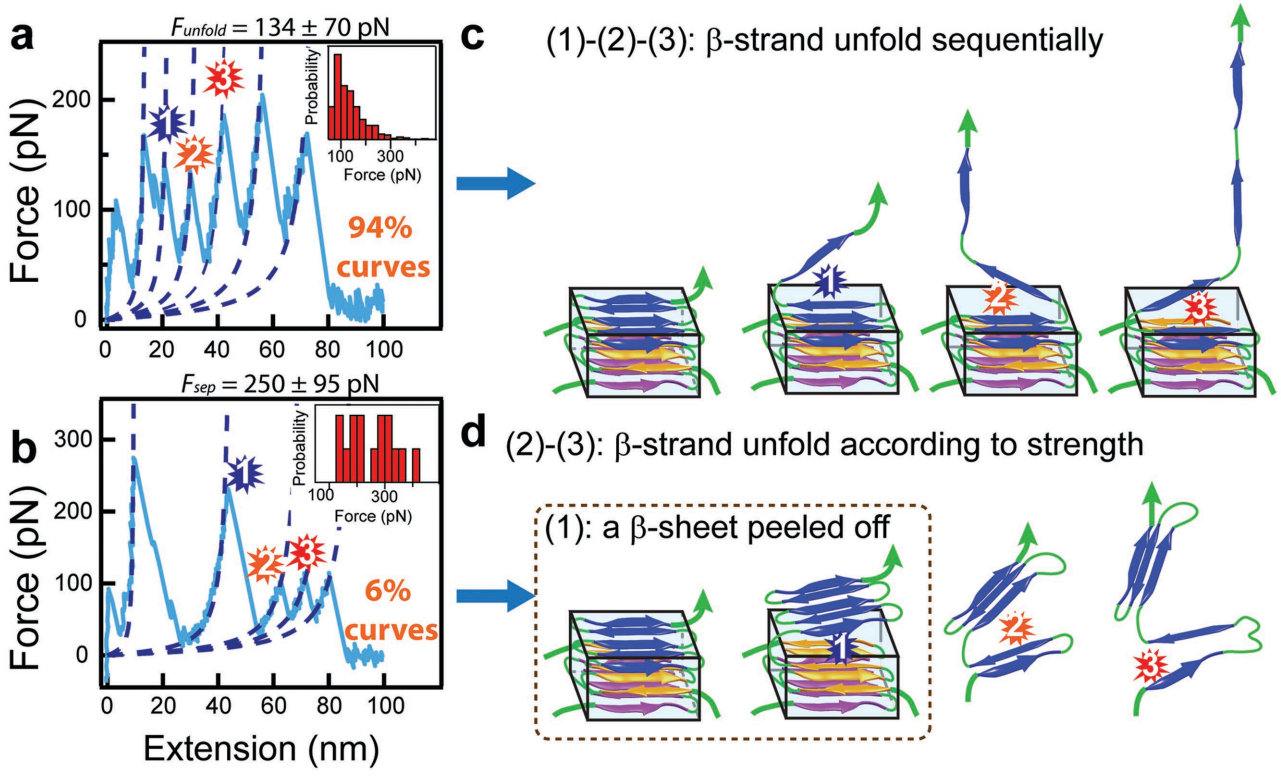

Figure 3. The scheme of two breakage pathways in the β-crystallite molecular network. a,b) Two types of force extension trajectories from AFM force measurements. The insets in (a) and (b) are the histograms of corresponding peak forces. The scheme of c) β-strands unfold sequentially out of a β-crystallite and d) a β-sheet is peeled off a β-crystallite, then the β-strands in the β-sheet unfold in the order of their strength.

on each β-strand within the β-sheet because they are connected in series. Thus, the weakest β-strand will be unzipped first, followed by others in the order of the strength (Figure 3d). This is analogous to the independent unfolding of domains as in the stretching of polyproteins like Titin,[26] and an upward trend in unfolding forces can be seen following a high-force unfolding event (Figure 3b).

Taking into account both the molecular interactions between amino acids and the size of each amino acid, we estimated the relative strength in the above two pathways, the possibility of observing each pathway, and the contour length change of peeling a β-sheet off a β-crystallite in the case of the fishnet structure. All estimations are in good agreement with the AFM results (see Note 2 in the Supporting Information for details), indicating that these nano-β-crystallites in regenerated BMCS fibrils are cross-linked to form the fishnet-like molecular networks (**Figure 4**a), other than the amyloid structure and the slab-segment structure. Similar force patterns are also observed for recombinant NAES fibrils (see Note 3, Supporting Information), suggesting the prevalence of the molecular fishnet structure among their fibrils. Therefore, the fishnet structure connected by the nano-β-crystallites turns out to be one of the most common characteristic structures in animal silk nanofibrils of different types.

As a matter of fact, the stacking and formation of β-crystallites are no doubt the center of the interests. It follows from the AFM results that both the unfolding forces and the contour length changes are quite broadly distributed (Figure S7, Supporting Information), and the variation is also observed within individual force–extension trajectories. This indicates that β-crystallites are most likely to be stacked by β-strands with varied length and strength, as illustrated by Figure 4b. The acquired information promises the "reconstruction" of β-crystallites as follows: silk fibrous protein molecular chains form some conventional intramolecular β-sheets.[12] The formation of a β-crystallite results from the folding and packing of the following sheets on the existing β-sheet as illustrated by 1 → 2 → 3 → 4 in Figure 4b. The subsequent piling up of β-sheets at the β-crystallite can be from other silk protein molecules. This process is controlled by nucleation when the initial β-sheets shown in Figure 4b1 serve as templates. Because the formation of silk fibrils is controlled by the nucleation of β-crystallites,[12] the occurrence of templates facilitates β-crystallite formation. In this way, the formation of β-crystallites gives rise to the cross-linking in the molecular fishnet structures of silk fibrils as pictured in Figure 4a.

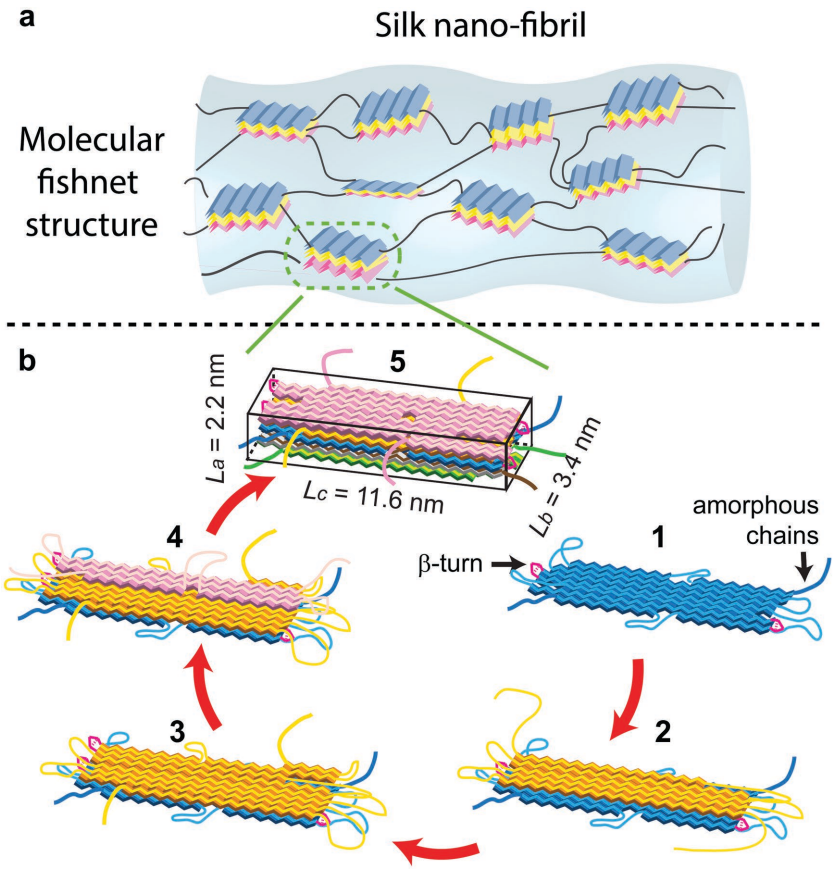

Figure 4. The molecular fishnet structure of a silk nanofibril and the proposed scheme for the formation of a β-crystallite. a) A scheme of the molecular fishnet structure of silk fibrils, where nano-β-crystallites are cross-linking by amorphous chains forming a fishnet structure. b) The formation of a β-crystallite: (1). A β-sheet is assembled by 7, 8 β-strands from the same silk fibroin molecule. (2). Taking 1 as a template, another fibroin molecule starts to form a β-sheet on it and becomes a nucleation of a new β-sheet layer. (3). A new layer on top of 1 forms. (4). More β-strands from other fibroin molecules are recruited to assemble additional β-sheet layers. (5). A β-crystallite consists of β-sheets from several silk fibroin molecules finally forms.

2.2. Nano Fishnet Structure Enhancement of the Mechanical Performance of Silk Fibers

We notice that the adoption of the nanocrystallite fishnet structures (Figure 4a) in animal silk fibrils has the most favored consequence in the macroscopic mechanical performance of silk fibers, in particular at the breaking points, due to the stronger and interconnective interactions. Unlike other arrangements, e.g., the slab-segment structure[11] and the amyloid structure,[24] this nano-"fishnet" can strengthen silk fibers by sharing external forces among the optimized network while keeping substantial elasticity of silk fibers. Such an arrangement allows the isolation of local breakages or defects and bypassing the loading stress around the broken points by the interconnectedness of the network (**Figure 5**a). In comparison, we applied Monte Carlo approach to simulate or numerical solutions to find the breaking stress for the following three structures: (1) the network structure of fishnet, (2) the bundle structure of no friction strings, and (3) the amyloid structure, we find the results can be fitted by a power law equation as

$$F_{BP} = F_0 + A \times n^{-B} \quad (1)$$

where, F_{BP}, n, F_0, A, and B are the breaking forces, the number of rows along the fibrils,

Adv. Funct. Mater. 2016,
DOI: 10.1002/adfm.201600813

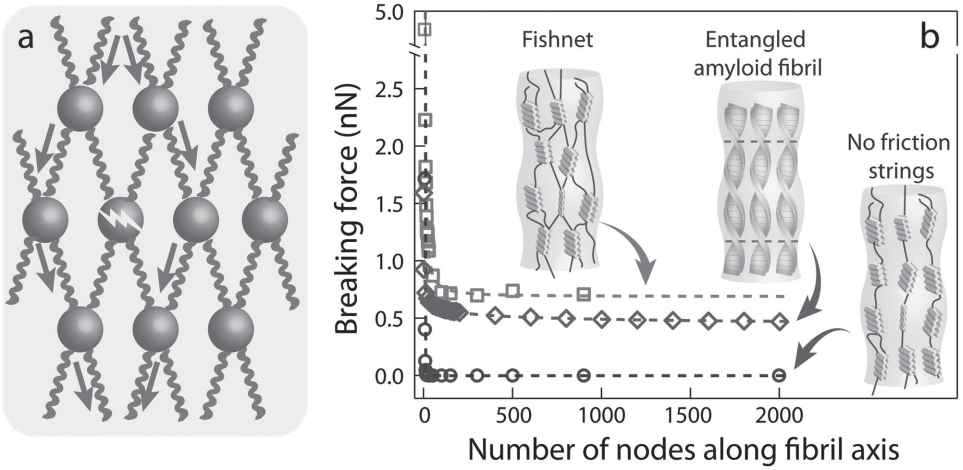

Figure 5. Modeling of the mechanical strength of the fishnet, no friction strings, and strengthened amyloid fibril structures of silk fibrils. a) The scheme of the molecular network in a silk fibril shows that the stress on the fibril can bypass the broken node (β-crystallite). The green arrows indicate the force along the fibroin molecules. b) The comparison of the mechanical strength by modeling three different molecular networks, and the breaking forces are plotted as functions of the length of the fibrils, i.e., the number of rows along fibrils axis. Here, □, ○, and ◊ are the modeling results and the corresponding curves are the fitting by the power law. Insets show the cartoon of the networks, where the blue blocks and orange squiggles represent β-crystallites/wires and amorphous chains/entanglements, respectively.

and three fitting parameters, respectively. Here, F_0 indicates the reserved force for very long fibrils. Comparing with other structures, the fishnet network gives rise to the toughest fibers (1.8 times or more). In addition, the fishnet model can stabilize long silk fibers at a substantially reserved mechanical strengthen (Figure 5b red square, and Note 5 (Supporting Information)).

In contrast, a bundle of independent β-crystallite strings show a much faster decay of the breaking force over the fibril length (Figure 5b, blue circle) and a remnant breaking force of zero for a long fibril. Concerning the amyloid network structure, we assume the entanglements at each segment size of ≈30 nm (see Note 5, Supporting Information). It turns out that the breaking force of such a fibril is right between a fishnet and a bundle of no friction strings, and its remnant breaking force is about 54% of that for a fishnet structure (Figure 5b). In other words, the entanglements of cross-linking the amyloid chains make such a pseudo and transient interconnecting network. Therefore, the adoption of the fishnet molecular network is natural selection in order to achieve the excel mechanical performance at the macroscopic.

2.3. Comparison between Spider Silk Fibers and Silkworm Silk Fibers: The Understanding Based upon the Fishnet Structure

As spider silk and silkworms silk fibers share the similar structure of fishnets, the question to be addressed is as to whether the similar structural characteristics of the two types of silk fibers would influence the mechanical performance in a similar way and why spider dragline fibers are of much high breaking stress than that of silkworm silk filaments. In this regard, we collected both spider dragline and silkworm silk fibers at different reeling rates (**Figure 6**a,b), and conducted the measurements of silk structures, i.e., small-angle X-ray scattering, FTIR, etc., and the corresponding mechanical strength.[7b]

As the β-crystallites, the nodes of networks, determine the strength of silk fibrous fishnets, the inter-β-sheet interaction should determine the strength of β-crystallites (or the nodes of networks). Therefore, stronger inter-β-interactions should enhance the strength of β-crystallites, which then gives rise to stronger silk fibers. It follows that the dependence between the breaking stress of silk fibers and the inter-β-sheet interaction from our analysis are in consistence with our observation. This gives rise to the fact that natural BMCS fibers possess the higher breaking stress than recombinant NAES fibers (Figure S10, Supporting Information). A similar analysis (Note 4, Supporting Information) indicates that the orientation of the β-crystallites in the fishnets of silk fibrils (the angle to the stress/fiber axis) influences the effect force to separate the β-sheets, therefore exerts a large impact on the toughness of the silk fibers. We carried out simulations (Note 4, Supporting Information) on the breaking stress of the "fishnet" fibers with varied ordering functions and densities of the β-crystallites. The simulated breaking stress shows a linear correlation with the measured one (Figure 6c), and the square of the Pearson's r is ≈0.956.

The above experiments verify the correlation between the ordering of the β-crystallites and the breaking stress of silk fibers (Figure 6d). Another important structural characteristic of fishnets is the mesh size (the square of correlation length) that should affect the strength of fishnets directly. Evidently, the smaller the mesh size (correlation length), the stronger the fishnets. This is in excellent agreement with Figure 6e, showing the dependence of the measured breaking stress of silkworm silk fibers on the density of the nodes (β-crystallites) in the fibers.

The aforementioned results have the following implications: (1) the basic structure of fishnets describes one of the main structural characteristics of both spider dragline and silkworm silk fibers. For instance, the correlation between the structural parameters, i.e., the strength and ordering of β-crystallites in the fibers and the mesh size of fishnets, and the breaking stress can be fitted by the same fitting trends (curves in Figure 6)

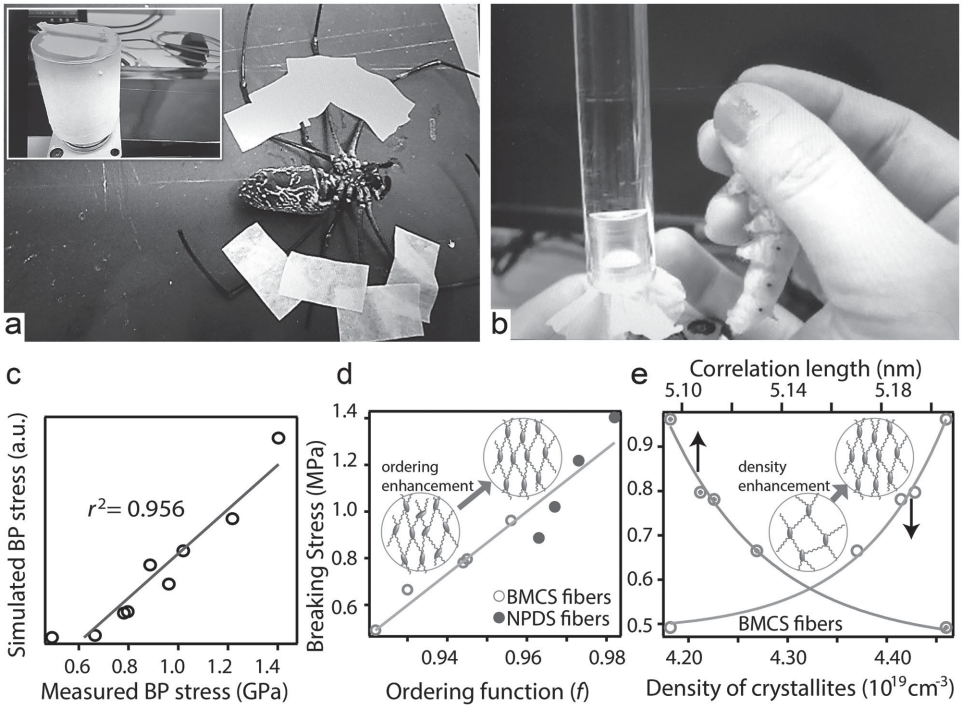

Figure 6. Dependency of the breaking stress on β-crystallite density and orientation. The photos show the experiments to draw fibers from immobilized a) spider *Nephila pilipes* and b) *Bombyx mori* silkworms. A computer-controlled motorized spindle (inset in (a)) allowed drawing fibers in a wide range of well-defined speeds, resulting in varied ordering and density of the β-crystallites in these fibrils.[7b] c) The simulated breaking stress show the same tendency as the breaking stress measured for silk fibers, including both BMCS and NPDS fibers, and the square of the Pearson's *r* is ≈0.956, The dependency of the measured breaking stress of BMCS (○) and NPDS (●) silk fibers on d) the alignment of β-crystallites in fibers (ordering function *f*) and e) the mesh size of fishnet networks/the density of β-crystallites. All the solid lines are fitted curves.

and explained well by the nano-fishnet model. (2) The higher breaking stress of spider dragline fibers in comparison with silkworm silk fibers can be attributed to the fact that spider dragline silk fibers have a better β-crystallite alignment or ordering and the smaller mesh size or correlation length of fishnets.

We notice that due to the absence of the fishnet structure, the fibers spun from soybean proteins, are never going to match the mechanical performance of both spider and silkworm silk fibers.[27] Our results clearly indicate the correlation between the fishnet structure of silk fibers with the mechanical performance of fibers. This should shed light on the design and synthesis of either protein or synthetic fibers of ultraperformance.

3. Conclusion

In summary, applying AFM force spectroscopy, the nanostructure of the protein network that comprises silk fibrils has been determined to be in line with the β-crystallite cross-linking network model, a molecular fishnet structure. Compared with other possible network structures, such a molecular fishnet of silk fibrils is the most optimized by nature for the mechanical performance of silk fibers. Based on the experimental results, the model for how the β-crystallites are assembled via molecular stacking and interchain molecular nucleation is proposed. Within the framework of this model, the limit of β-crystallites breakage determines the strength of silk fibers, which is determined by the β-conformation forming residues. It then follows that the inter-β-sheet interactions and the orientation of β-crystallites are the key factors determining the stability of β-crystallites, while the variation in the density of β-crystallites can significantly change the mechanical performance of silk fibers. In general speaking, the results are well captured by the soft matter mesoscopic structure-performance Yin-Yang sphere model (Figure 1).

4. Experimental Section

Sample Preparation: Silk fibroin solution was obtained by dissolving the middle division of the gland of the fifth instar silkworm *B. mori* in the deionized (DI) water after the sericin was completely washed away. Obtained stock solution was diluted to 0.1 mg mL^{-1} and kept in tube at room temperature until the final silkworm silk fibrils were fully formed (regenerated *Bombyx mori* (*B. mori*) cocoon silk fibrils solution). The whole process usually took around one to two weeks. Recombinant spider eggcase protein was synthesized resembling the sequences of the type 1 repetitive domains of the tubuliform spidroin from golden web spider (*N. antipodiana*), following the previous procedure.[28] The synthesized protein consisted of four tandem repeats and the sequences of each repeats were shown in Figure S1 (Supporting Information). The structural transition into β-sheet for the recombinant spider eggcase silk proteins occurred at ≈75 °C,[28] so the recombinant spider eggcase silk protein solution (0.1 mg mL^{-1}) was incubated at 90 °C and circular dichroism was used to monitor the structural changes of the protein solution to ensure that the transition was completed and the final recombinant spider NAES fibrils were fully formed.

After the silk fibrils were fully formed, a small drop of the silk protein solution was deposited onto the 3-aminopropyl triethoxysilane treated mica and allowed to be incubated for 5 min. The sample was then

DOI: 10.1002/adfm.201600813

washed with the DI water and was dried with a stream of nitrogen gas before the AFM imaging or AFM force spectroscopy experiment.

The sponge samples for XRD were prepared by freeze drying. The fibril solution was first frozen with liquid nitrogen and then lyophilized at –80 °C for 3 d using a Labconco FreeZone 2.5 plus drier. The powder samples of *B. mori* silk fibers for XRD were prepared following the procedure as described before.[29]

The alignment of the regenerated BMCS fibrils was achieved by placing a droplet of fibril solution between the wax ends of two glass capillaries and allowing it to dry at room temperature. The procedure was repeated until the aligned regenerated BMCS sample reached a diameter of ≈2 mm for later XRD experiment. To investigate the effect of the shear on the chain arrangement of the β-nanocrystallites, shear force was applied on the silk fibroin solution through circular agitation until white flocs emerged. The white flocs were collected and aligned for later characterization by XRD.

Mechanical Tests: Instron Micro Tester (Model 5848) was used to measure the mechanical properties of silks. The force resolution was 0.5% of indicated load, the position resolution was 0.02 µm, and strain rate was 50% per minute. The whole tests were performed at 22 °C and the relative humidity was 60%.

XRD: Diffraction data were collected using Rigaku FR-E high brilliance X-ray generator with Cu-Kα radiation (k = 0.15418 nm). The sample-detector distance was 50 mm, and the exposure time was 50 s.

FTIR: FTIR spectra were collected using Nicolet 380 FTIR spectrometer at a resolution of 4 cm^{-1} averaging over 256 scans.

Seeds Preparation: The seeds for the acceleration of the β-conformation growth experiments were prepared by applying ultrasonification on 0.1 mg mL^{-1} mature fibroin solution (in which fibroin molecules had mostly assembled to the nanofibrils) for 70 min at 150 W with repeated pulses of on (2 s) and off (8 s).

Fluorescence Measurement: Dye binding assays were performed at 5 µg mL^{-1} peptide, diluted from the 0.1 mg mL^{-1} fibroin solution into deionized water containing the Thioflavin T dyes. Fluorescence measurements were performed using Cary Eclipse fluorescence spectrophotometer (Varian) with a 1.0 cm path length quartz cell. The mixed solution samples were excited at 442 nm, and data were recorded at 485 nm, with a bandwidth of 10 nm for both the excitation and emission monochromators. Blanks (deionized water containing dye) were always subtracted under the same experimental conditions.

AFM Imaging and Force Spectroscopy Experiment: AFM imaging in air was carried on Veeco Dimension 3000 using tapping mode. Cantilevers for AFM imaging were bought from Veeco with a spring constant of 40 N m^{-1}. AFM force spectroscopy was conducted in a 10×10^{-3} M $CaCl_2$ solution on JPK Nanowizard II, while the silicon nitride cantilevers with a spring constant of ≈23 pN nm^{-1} was bought from Applied NanoStructures Inc. In the force spectroscopy experiment, imaging was first conducted to locate the position of the fibrils. Then the AFM tip approached the fibril surface at a velocity of 600 nm s^{-1}, and was pressed against the fibril with a force of 450 pN for 1 s before retraction from the surface with the same speed. Occasionally, a single molecule in a single silk fibril was mechanically stretched between the tip and substrate. The force–extension curves were recorded. This procedure was repeated many times, and the pickup rate, the percentage of force–extension curves showing unfolding events of proteins, was lower than 2%. The force peaks from these curves were selected for further analysis using usual criteria for separation of multichain and single chain events.[20,30]

Data Analysis: All the AFM images were processed in the Nanoscope or WSxM software. The force spectra were processed with home-written codes in Labview. The force versus extension trajectories were fit by the worm-like chain model,[26,31] with a persistence length of 0.4 nm and an adjustable contour length. For each unfolding event, the contour length change, ΔL, and unfolding peak force was recorded. The total events number was 766 for regenerated BMCS and 625 for recombinant NAES fibrils, respectively. All the errors in the text referred to the standard deviation. The force–extension trajectories with the general upward trend in the unfolding forces (≥3 peaks) were considered as the separation of the β-sheet plate.

Supporting Information

Supporting Information is available from the Wiley Online Library or from the author.

Acknowledgements

The authors thank Prof. Lim CT and GEM4 at Department of Bioengineering, National University of Singapore, for providing the machine for atomic force spectroscopy. This study was supported by "111" Project (B16029), National Nature Science Foundation of China (No. U1405226), Fujian Provincial Department of Science & Technology (2014H6022), and the 1000 Talents Program from Xiamen University.

Received: February 16, 2016
Revised: May 3, 2016
Published online:

[1] Y. Y. Diao, X. Y. Liu, G. W. Toh, L. Shi, J. Zi, *Adv. Funct. Mater.* **2013**, *23*, 5373.
[2] N. Lin, X. Y. Liu, *Chem. Soc. Rev.* **2015**, *44*, 7881.
[3] J. Hemminger, G. Crabtree, M. Kastner, *A Report from the Basic Energy Sciences Advisory Committee, Tech. Rep*, **2012**, 1601.
[4] a) N. Du, Z. Yang, X. Y. Liu, Y. Li, H. Y. Xu, *Adv. Funct. Mater.* **2011**, *21*, 772; b) D. T. Grubb, L. W. Jelinski, *Macromolecules* **1997**, *30*, 2860; c) C. Riekel, B. Madsen, D. Knight, F. Vollrath, *Biomacromolecules* **2000**, *1*, 622; d) A. H. Simmons, C. A. Michal, L. W. Jelinski, *Science* **1996**, *271*, 84; e) R. Valluzzi, H. J. Jin, *Biomacromolecules* **2004**, *5*, 696; f) J. D. Van Beek, S. Hess, F. Vollrath, B. H. Meier, *Proc. Natl. Acad. Sci. USA* **2002**, *99*, 10266; g) L. Eisoldt, A. Smith, T. Scheibel, *Mater. Today* **2011**, *14*, 80; h) J. E. Trancik, J. T. Czernuszka, F. I. Bell, C. Viney, *Polymer* **2006**, *47*, 5633; i) S. Putthanarat, N. Stribeck, S. A. Fossey, R. K. Eby, W. W. Adams, *Polymer* **2000**, *41*, 7735; j) Y. Shen, M. A. Johnson, D. C. Martin, *Macromolecules* **1998**, *31*, 8857; k) T. Lefevre, M. E. Rousseau, M. Pezolet, *Biophys. J.* **2007**, *92*, 2885.
[5] Z. Z. Shao, F. Vollrath, *Nature* **2002**, *418*, 741.
[6] a) S. Lapiodot, S. Meirovitch, S. Sharon, A. Heyman, D. L. Kaplan, O. Shoseyov, *Nanomedicine (London, UK)* **2012**, *7*, 1409; b) G. H. Li, H. Liu, T. D. Li, J. Y. Wang, *Mater. Sci. Eng., C* **2012**, *32*, 627; c) F. G. Omenetto, D. L. Kaplan, *Science* **2010**, *329*, 528.
[7] a) M. Heim, D. Keerl, T. Scheibel, *Angew. Chem., Int. Ed.* **2009**, *48*, 3584; b) N. Du, X. Y. Liu, J. Narayanan, L. A. Li, M. L. M. Lim, D. Q. Li, *Biophys. J.* **2006**, *91*, 4528; c) A. Tarakanova, M. J. Buehler, *JOM* **2012**, *64*, 214.
[8] a) G. Q. Xu, L. Gong, Z. Yang, X. Y. Liu, *Soft Matter* **2014**, *10*, 2116; b) A. T. Nguyen, Q. L. Huang, Z. Yang, N. Lin, G. Xu, X.-Y. Liu, *Small*, **2015**, *11*, 1039.
[9] T. Asakura, Y. Suzuki, Y. Nakazawa, G. P. Holland, J. L. Yarger, *Soft Matter* **2013**, *9*, 11440.
[10] a) S. Keten, Z. P. Xu, B. Ihle, M. J. Buehler, *Nat. Mater.* **2010**, *9*, 359; b) X. Wu, X. Y. Liu, N. Du, G. Q. Xu, B. W. Li, *Appl. Phys. Lett.* **2009**, *95*, 093703.
[11] E. Oroudjev, J. Soares, S. Arcdiacono, J. B. Thompson, S. A. Fossey, H. G. Hansma, *Proc. Natl. Acad. Sci. USA* **2002**, *99*, 9606.
[12] A. T. Nguyen, Q. L. Huang, Z. Yang, N. Lin, G. Xu, X. Y. Liu, *Small* **2015**, *11*, 1039.
[13] a) E. Carretti, M. Bonini, L. Dei, B. H. Berrie, L. V. Angelova, P. Baglioni, R. G. Weiss, *Acc. Chem. Res.* **2010**, *43*, 751; b) G. Xu, L. Gong, Z. Yang, X. Liu, *Soft Matter* **2014**, *10*, 2116.
[14] a) C. A. E. Hauser, S. Maurer-Stroh, I. C. Martins, *Chem. Soc. Rev.* **2014**, *43*, 5326; b) J. J. Panda, V. S. Chauhan, *Polym. Chem.* **2014**, *5*, 4418; c) K. Matsuurua, *RSC Adv.* **2014**, *4*, 2942.

[15] a) L. R. Volpatti, T. P. J. Knowles, *J. Polym. Sci., Part B: Polym. Phys.* **2014**, *52*, 281; b) S. B. Xiao, S. J. Xiao, F. Grater, *Phys. Chem. Chem. Phys.* **2013**, *15*, 8765.
[16] a) L. N. Zhao, L. Y. Lu, L. Y. Chew, Y. G. Mu, *Int. J. Mol. Sci.* **2014**, *15*, 12631; b) F. Meersman, R. Q. Cabrera, P. F. McMillan, V. Dmitriev, *High Pressure Res.* **2009**, *29*, 665.
[17] a) A. Abelein, J. P. Abrahams, J. Danielsson, A. Graslund, J. Jarvet, J. H. Luo, A. Tiiman, S. Warmlander, *J. Biol. Inorg. Chem.* **2014**, *19*, 623; b) R. Tycko, R. B. Wickner, *Acc. Chem. Res.* **2013**, *46*, 1487.
[18] a) R. Tycko, in *Annual Review of Physical Chemistry*, Vol. *62* (Eds: S. R. Leone, P. S. Cremer, J. T. Groves, M. A. Johnson), Annual Reviews, Palo Alto **2011**, p. 279; b) M. Weingarth, M. Baldus, *Acc. Chem. Res.* **2013**, *46*, 2037.
[19] a) J. J. Li, C. M. Yip, *Biochim. Biophys. Acta, Biomembr.* **2013**, *1828*, 2272; b) H. Hiramatsu, *Yakugaku Zasshi – J. Pharm. Soc. Jpn. (English)* **2014**, *134*, 1013.
[20] M. Carrion-Vazquez, A. F. Oberhauser, T. E. Fisher, P. E. Marszalek, H. B. Li, J. M. Fernandez, *Prog. Biophys. Mol. Biol.* **2000**, *74*, 63.
[21] a) E. Drolle, F. Hane, B. Lee, Z. Leonenko, *Drug Metab. Rev.* **2014**, *46*, 207; b) M. Sullivan, S. Keten, *J. Appl. Mech.-Trans. ASME* **2013**, *80*, 061010; c) M. Schleeger, C. C. VandenAkker, T. Deckert-Gaudig, V. Deckert, K. P. Velikov, G. Koenderink, M. Bonn, *Polymer* **2013**, *54*, 2473; d) H. Shulha, C. W. P. Foo, D. L. Kaplan, V. V. Tsukruk, *Polymer* **2006**, *47*, 5821; e) W. K. Zhang, Q. B. Xu, S. Zou, H. B. Li, W. Q. Xu, X. Zhang, Z. Z. Shao, M. Kudera, H. E. Gaub, *Langmuir* **2000**, *16*, 4305.
[22] a) J. Adamcik, C. Lara, I. Usov, J. S. Jeong, F. S. Ruggeri, G. Dietler, H. A. Lashuel, I. W. Hamley, R. Mezzenga, *Nanoscale* **2012**, *4*, 4426; b) C. Lara, S. Gourdin-Bertin, J. Adamcik, S. Bolisetty, R. Mezzenga, *Biomacromolecules* **2012**, *13*, 4213; c) K. Sweers, K. Van der Werf, M. Bennink, V. Subramaniam, *Nanoscale Res. Lett.* **2011**, *6*, 1.
[23] a) D. E. Dunstan, P. Hamilton-Brown, P. Asimakis, W. Ducker, J. Bertolini, *Soft Matter* **2009**, *5*, 5020; b) A. Karsai, Z. Martonfalvi, A. Nagy, L. Grama, B. Penke, M. S. Z. Kellermayer, *J. Struct. Biol.* **2006**, *155*, 316; c) M. S. Z. Kellermayer, L. Grama, A. Karsai, A. Nagy, A. Kahn, Z. L. Datki, B. Penke, *J. Biol. Chem.* **2005**, *280*, 8464; d) J. F. Smith, T. P. J. Knowles, C. M. Dobson, C. E. MacPhee, M. E. Welland, *Proc. Natl. Acad. Sci. USA* **2006**, *103*, 15806.
[24] J. J. Wiltzius, S. A. Sievers, M. R. Sawaya, D. Cascio, D. Popov, C. Riekel, D. Eisenberg, *Protein Sci.* **2008**, *17*, 1467.
[25] P. D. Bosshart, I. Iordanov, C. Garzon-Coral, P. Demange, A. Engel, A. Milon, D. J. Muller, *Structure* **2012**, *20*, 121.
[26] M. Rief, M. Gautel, F. Oesterhelt, J. M. Fernandez, H. E. Gaub, *Science* **1997**, *276*, 1109.
[27] X. F. Zhang, B. G. Min, S. Kumar, *J. Appl. Polym. Sci.* **2003**, *90*, 716.
[28] Z. Lin, W. D. Huang, J. F. Zhang, J. S. Fan, D. W. Yang, *Proc. Natl. Acad. Sci. USA* **2009**, *106*, 8906.
[29] E. S. Gil, J. A. Kluge, D. N. Rockwood, R. Rajkhowa, L. J. Wang, X. G. Wang, D. L. Kaplan, *J. Biomed. Mater. Res., Part A* **2011**, *99A*, 16.
[30] W. Zhang, X. Zhang, *Prog. Polym. Sci.* **2003**, *28*, 1271.
[31] T. E. Fisher, P. E. Marszalek, A. F. Oberhauser, M. Carrion-Vazquez, J. M. Fernandez, *J. Physiol.-London* **1999**, *520*, 5.

Adv. Funct. Mater. **2016**,
DOI: 10.1002/adfm.201600813